UCLA

UCLA Previously Published Works

Title

Characterization of a Mycobacterium tuberculosis Nanocompartment and Its Potential Cargo Proteins*

Permalink

https://escholarship.org/uc/item/3n04d8wj

Journal

Journal of Biological Chemistry, 289(26)

ISSN

0021-9258

Authors

Contreras, Heidi
Joens, Matthew S
McMath, Lisa M
et al.

Publication Date

2014-06-01

DOI

10.1074/jbc.m114.570119

Peer reviewed

Characterization of a *Mycobacterium tuberculosis* Nanocompartment and Its Potential Cargo Proteins[*]

Heidi Contreras[‡], Matthew S. Joens[§1], Lisa M. McMath[‡], Vincent P. Le[‡], Michael V. Tullius[¶], Jaqueline M. Kimmey[¶], Neda Bionghi[¶], Marcus A. Horwitz[¶], James A. J. Fitzpatrick[§1], and Celia W. Goulding[‡||2]

From the Departments of [‡]Molecular Biology and Biochemistry and [||]Pharmaceutical Sciences, University of California, Irvine, California 92697, the [§]Waitt Advanced Biophotonics Center, Salk Institute for Biological Studies, La Jolla, California 92037, and the [¶]Division of Infectious Diseases, Department of Medicine, School of Medicine, UCLA, Los Angeles, California 90095

Background: *Mycobacterium tuberculosis* has a probable nanocompartment (Mt-Enc).
Results: Mt-Enc self-assembles into a 60-subunit cage that encapsulates enzymes via their C-terminal tails, which remain active within Mt-Enc.
Conclusion: Cargo proteins are potentially involved in host oxidative stress response, suggesting that enzyme encapulation may be a mechanism to evade host immune assault.
Significance: Mt-Enc may be utilized as a novel therapeutic delivery mechanism.

Mycobacterium tuberculosis **has evolved various mechanisms by which the bacterium can maintain homeostasis under numerous environmental assaults generated by the host immune response.** *M. tuberculosis* **harbors enzymes involved in the oxidative stress response that aid in survival during the production of reactive oxygen species in activated macrophages. Previous studies have shown that a dye-decolorizing peroxidase (DyP) is encapsulated by a bacterial nanocompartment, encapsulin (Enc), whereby packaged DyP interacts with Enc via a unique C-terminal extension.** *M. tuberculosis* **also harbors an encapsulin homolog (CFP-29, Mt-Enc), within an operon with** *M. tuberculosis* **DyP (Mt-DyP), which contains a C-terminal extension. Together these observations suggest that Mt-DyP interacts with Mt-Enc. Furthermore, it has been suggested that DyPs may function as either a heme-dependent peroxidase or a deferrochelatase. Like Mt-DyP,** *M. tuberculosis* **iron storage ferritin protein, Mt-BfrB, and an** *M. tuberculosis* **protein involved in folate biosynthesis, 7,8-dihydroneopterin aldolase (Mt-FolB), have C-terminal tails that could also interact with Mt-Enc. For the first time, we show by co-purification and electron microscopy that mycobacteria via Mt-Enc can encapsulate Mt-DyP, Mt-BfrB, and Mt-FolB. Functional studies of free or encapsulated proteins demonstrate that they retain their enzymatic activity within the Mt-Enc nanocompartment. Mt-DyP, Mt-FolB, and Mt-BfrB all have antioxidant properties, suggesting that if these proteins are encapsulated by Mt-Enc, then this nanocage may play a role in the** *M. tuberculosis* **oxidative stress response. This report provides initial structural and biochemical clues regarding the molecular mechanisms that utilize compartmentalization by which the mycobacterial cell may aid in** detoxification of the local environment to ensure long term survival.

The etiologic agent of tuberculosis, *Mycobacterium tuberculosis*, infects ~11.1 million people per year, resulting in over 1.3 million deaths worldwide (1). With the emergence of *M. tuberculosis* strains resistant to the major anti-tuberculosis therapies, the discovery of novel drug targets is imperative to triumph over tuberculosis infection. Deciphering the complicated biology of *M. tuberculosis*, which has both active and latent forms, will aid in the discovery of new therapeutics to combat this highly successful pathogen.

In mammalian cells, exosomes are secreted vesicles proposed to be involved in mediating the adaptive immune response (2, 3). Mycobacterial proteins have been discovered in exosomes of cells infected with *M. tuberculosis*. One mycobacterial protein identified within exosomes was a 29-kDa culture filtrate protein (CFP-29, Rv0798c) (4), reported to be secreted (5), although lacking a signal peptide. CFP-29 has 58% amino acid identity to *Brevibacterium linens* M18 linocin protein (also known as encapsulin, Bl-Enc)[3] (5), implying that CFP-29 is an *M. tuberculosis* encapsulin homolog (Mt-Enc). Throughout the remainder of this work, CFP-29 (Rv0798c) will be referred to as Mt-Enc. Additionally, the gene encoding Bl-Enc is within a two-gene operon containing a gene encoding for a dye-decolorizing peroxidase (Bl-DyP) with a ~25-amino acid C-terminal extension (Fig. 1*A*). The crystal structure of a close homolog of Bl-Enc, *Thermotoga maritima* encapsulin (Tm-Enc), has been determined, revealing a 60-subunit icosahedral nanocompartment (6). Electron microscopy (EM) shows that coexpression of Bl-DyP and Bl-Enc results in encapsulation of Bl-DyP within the Bl-Enc nanocage, where encapsulation of Bl-DyP is abolished upon truncation of its C-terminal extension (6). Finally, a

[3] The abbreviations used are: Enc, encapsulin; DyP, dye-decolorizing peroxidase; δ-ALA, δ-aminolevulinic acid; PPIX, protoporphyrin IX; ABTS, 2,2′-azino-bis(3-ethylbenzothiazoline-6-sulfonic acid; FAS, ferrous ammonium sulfate; MCP, microcompartment.

A

C-terminal extension

Mt-DyP	311	–LPQAATPTLAAGSLSIGSLKGSPR	335	
Mt-BfrB	162	EEVDVAPAASGAPHAAGGRL-----	181	
Mt-FolB	118	---RR-GGRGWVVP-AGGAV-----	133	
Bl-DyP	343	QTAEEAARDTSDGSLGIGSLKRSRQ	367	
Tm-Flp	93	---EIEEETSGGSENTGGDLGIRKL	114	
Ho-Ald	245	---RDDLVRIVREELVRALA-----	261	

B

Mt-FolB

C-terminal extension

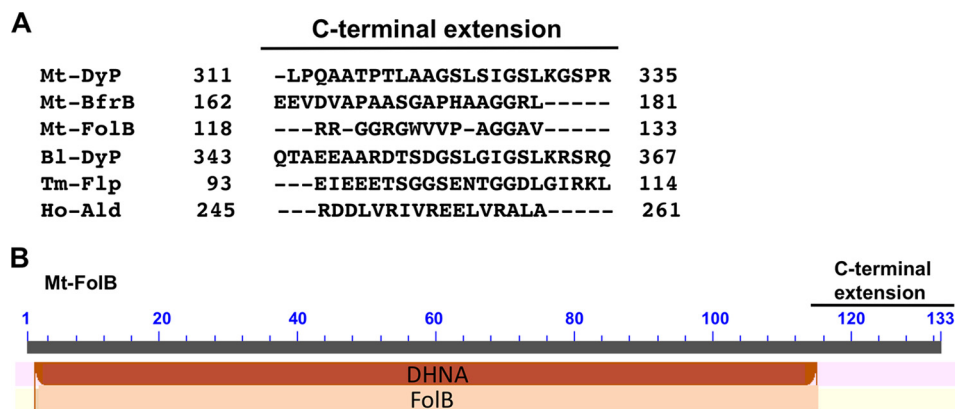1   20   40   60   80   100   120   133

DHNA
FolB

FIGURE 1. **C-terminal extensions of potential Mt-Enc protein cargos.** *A*, C-terminal extension residue sequences of Mt-DyP, Mt-BfrB, and Mt-FolB beyond what is seen in homologs that are not encapsulated as well as *B. linens* DyP (Bl-DyP (6)), *T. maritima* ferritin-like protein (Tm-Flp (6)), and a putative *H. ochraceum* aldolase (Ho-Ald (59)) thought to be encapsulated by its C-terminal tail to BMCs. *B*, the *top numbered gray line* represents Mt-FolB residues, and the *brown* and *light orange boxes* represent conserved 7,8-dihydroneopterin aldolase (*DHNA*) and FolB domains, respectively, from various organisms generated by the Conserved Domain Database (63).

search across bacterial genomes demonstrates that genes encoding for Enc are usually in two-gene operons with a gene encoding for either DyP or ferritin-like proteins, all with predominately hydrophobic C-terminal extensions (Fig. 1*A*) (6). These observations suggest that Enc proteins compartmentalize DyP or ferritin-like proteins via their C-terminal tails. Notably, both DyPs and ferritin proteins possess antioxidant properties (7, 8).

Mt-Enc, the only homolog of Enc in *M. tuberculosis*, is part of a two-gene operon with the gene for a DyP-like peroxidase (Mt-DyP, Rv0799c), where Mt-DyP contains a C-terminal extension similar to Bl-DyP (Fig. 1*A*). DyP-type peroxidases are a novel family of fungal and bacterial heme-dependent peroxidases that can oxidize lignin and anthraquinone dyes in the presence of H_2O_2 (9, 10). However, the *Escherichia coli* DyP ortholog, Ec-YfeX, was proposed to possess deferrochelatase activity, where Ec-YfeX can catalyze the extraction of iron from heme without cleavage of the tetrapyrrole ring (11), although in a parallel study, Ec-YfeX was demonstrated to be a heme-dependent peroxidase with no detectable deferrochelatase activity (12). If Mt-DyP is a heme-dependent peroxidase, then Mt-DyP may protect *M. tuberculosis* against host oxidative assault by H_2O_2.

Notably, two other *M. tuberculosis* proteins have aliphatic C-terminal extensions beyond what is seen in other bacterial homologs and similar to Mt-DyP, suggesting that these proteins may also be cargo proteins for Mt-Enc. Mt-BfrB, one of the two iron storage ferritin proteins within *M. tuberculosis*, has a C-terminal tail (Fig. 1*A*) and has displayed antioxidant properties (13, 14). In addition, an enzyme involved in folate metabolism, 7,8-dihydroneopterin aldolase (Mt-FolB), also has an aliphatic C-terminal extension (Fig. 1*B*). In a previous study, Mt-FolB structure determination shows that this C-terminal extension is disordered, and Mt-FolB enzymatic activity is independent of the C-terminal tail. Furthermore, its substrate has also been implicated in *M. tuberculosis* resistance to oxidative stress (15–17).

Herein we describe the Mt-Enc encapsulation of three different *M. tuberculosis* enzymes, Mt-DyP, Mt-BfrB, and Mt-FolB, all of which possess antioxidant properties. We show by EM

that Mt-Enc can encapsulate *M. tuberculosis* cargo enzymes and show by biochemical analyses that the enzymes remain active within the Mt-Enc nanocompartment. We also carried out preliminary characterization of Mt-DyP and suggest that it is primarily a heme peroxidase. To our knowledge, this study provides the initial report into mycobacterial compartmentalization of enzymes, whereby protein encapsulation by Mt-Enc may function to combat oxidative stress within the human host.

MATERIALS AND METHODS

Cloning

The *M. tuberculosis* genes encoding proteins Mt-BfrA (*Rv1876*), Mt-BfrB (*Rv3841*), Mt-DyP (*Rv0799c*), Mt-Enc (*Rv0798c*), and Mt-FolB (*Rv3607c*) were PCR-amplified from *M. tuberculosis* H37Rv genomic DNA using the KOD HotStart Polymerase Kit (Novagen) with 5′ and 3′ primers (MWG Operon) containing specific restriction sites to generate either a C-terminal polyhistidine tag (His tag) or a tagless protein. PCR products were ligated into pCR-BluntII-TOPO (Invitrogen) and then transformed into *E. coli* OneShot TOP10 cells (Invitrogen). Double digestions with specific restriction enzymes were performed from each vector of choice. Excised genes were ligated into the appropriate linearized pET vector and transformed into *E. coli* BL21-Gold (DE3) cells (Novagen). Each final construct was verified by DNA sequencing using T7 promoter and reverse primers (Laguna Scientific).

Overexpression and Purification of M. tuberculosis Proteins

Proteins were expressed from plasmids alone or in combination with one another, using *E. coli* BL21 Gold (DE3) cells. The following concentrations of antibiotics to the media were added where appropriate: kanamycin (30 μg/ml) and ampicillin (50 μg/ml). Cells harboring expression vector(s) were grown aerobically at 37 °C in LB medium containing the appropriate antibiotic(s). Protein expression was induced at A_{600} ~0.8 by the addition of isopropyl-β-D-thiogalactopyranoside (1 mM). Cells were harvested after 4 h of induction (apart from Mt-Enc and proteins in complex with Mt-Enc, which were induced overnight at 18 °C) by centrifugation at 5100 × *g* for 20 min. Additionally, only where indicated cultures express-

ing Mt-Enc·DyP were supplemented with 0.7 mM δ-aminolevulinic acid (δ-ALA) at the time of induction.

Harvested cell pellets were resuspended in 20 ml of Buffer A (50 mM Tris-HCl, pH 7.4, 350 mM NaCl, 10 mM imidazole, and 10% glycerol), followed by the addition of PMSF and hen egg white lysozyme. Pellets containing Mt-Enc and proteins in complex with Mt-Enc were resuspended in Buffer A containing 0.2% lauryldimethylamine oxide for solubilization. Cells were disrupted by sonication, clarified by centrifugation at 18,000 × g for 30 min at 4 °C, and syringe-filtered (1-μm pore size) for removal of cell debris. The clarified cell lysate was then loaded onto a 5-ml Ni^{2+}-charged HisTrap column (GE Healthcare) pre-equilibrated with Buffer A. The protein(s) was eluted with a linear gradient of 10–500 mM imidazole (100 ml). Proteins that co-purify with Mt-Enc elute at a higher imidazole concentration (>250 mM imidazole). Eluted fractions were collected, analyzed by SDS-PAGE, and concentrated using Amicon concentrators with the appropriate molecular weight cut-off (Millipore, Bedford, MA). Mt-DyP and Mt-BfrB were further purified on a Superdex 200 HiLoad 16/60 gel filtration chromatography column (GE Healthcare) utilizing 50 mM Tris-HCl, pH 7.4, and 150 mM NaCl, and their respective molecular weights were calculated using molecular weight standards (Bio-Rad). Mt-BfrB was dialyzed into 20 mM Tris-HCl, pH 8.0, and 10 mM NaCl and purified by ion exchange (5 ml; HiTrap™ Q HP, GE Healthcare). The protein was eluted with a linear gradient of 0.01–1.0 M NaCl (100 ml); the purified protein eluted between 400 and 600 mM NaCl. Protein concentration was determined by UV-visible spectroscopy, utilizing molar extinction coefficients at 280 nm as predicted by the program Protein Calculator (Scripps) or as determined by either a modified Lowry (18) or Bradford (19) assay using bovine serum albumin as a standard.

Electron Microscopy

Samples were negatively stained as follows. Ultrathin carbon and silicon monoxide grids (Ted Pella catalogue nos. 01824 and 01829, respectively) were prepared by removing the Formvar backing by dipping the grids in 100% chloroform for 10 s and glow-discharging them for 30 s (Leica SCD500, Leica, Vienna). Samples were diluted 1:10 in buffer, and 5 μl of this was placed on a grid and immediately washed twice in double-distilled H$_2$O, followed by a 1-min incubation in 1% uranyl acetate. Excess stain was then aspirated off, and the grid was allowed to dry at room temperature. Following negative staining, the grids were imaged on a Zeiss Libra 120 PLUS EF-TEM (Carl Zeiss).

Generation and Characterization of MtbΔmbtB Strains Deficient in Mt-DyP, MhuD, or Both Mt-DyP and MhuD

MtbΔ*mbtB*, a mycobactin-deficient mutant of *M. tuberculosis*, was used as the parental strain to construct the double and triple mutants MtbΔ*mbtB*Δ*dyP*, MtbΔ*mbtB*Δ*mhuD*, and MtbΔ*mbtB*Δ*mhuD*Δ*dyP* via specialized transduction as described previously (20). To generate the MtbΔ*mbtB*Δ*mhuD* mutant, we constructed an allelic exchange substrate by cloning a 1.9-kb PCR product, including the entire *mhuD* gene and flanking regions, and then replacing 222 nucleotides of the *mhuD* gene (encoding amino acids 10–85 of the

105-amino acid MhuD protein) with an apramycin resistance cassette, using essentially the same strategy described previously for construction of MtbΔ*mbtB*Δ*mmpL11* and MtbΔ*mbtB*Δ*Rv0203* (20). To generate the Δ*dyP* mutants, MtbΔ*mbtB*Δ*dyP* and MtbΔ*mbtB*Δ*mhuD*Δ*dyP*, we first inserted an 849-nucleotide in-frame, unmarked deletion of *dyP* (encoding amino acids 21–303 of the 335-amino acid DyP protein) flanked by a hygromycin resistance gene and sacB cassette (hyg-sacB) into the *dyP* region of the chromosome by specialized transduction. In a second step, we passaged hygromycin-resistant clones that were sensitive to sucrose (due to expression of sacB) in the absence of hygromycin to allow for recombination to occur between homologous regions flanking the hyg-sacB cassette (eliminating the hyg-sacB cassette from the chromosome and leaving just the unmarked Δ*dyP* mutation) and then plated them on 7H10 plates containing 2% sucrose. Sucrose-resistant clones were confirmed to have lost hygromycin resistance by plating on 7H10 plates with and without hygromycin. All mutants were confirmed to have the correct genotype by PCR.

Heme utilization experiments were carried out as described previously (20), except 7H9 growth medium was supplemented with 10% Oleic Acid, Albumin, Dextrose, Catalase (OADC) and 0.01% tyloxapol (7H9-OADC-TLX). Log phase bacteria were inoculated at an initial A_{750} of 0.0005 into 30 ml of 7H9-OADC-TLX containing no supplement, 0.2 μM heme, or 10 ng/ml mycobactin J and grown for 21 days until the growth of all strains had plateaued in the presence of mycobactin J. The growth of the double and triple mutants (MtbΔ*mbtB*Δ*dyP*, MtbΔ*mbtB*Δ*mhuD*, and MtbΔ*mbtB*Δ*mhuD*Δ*dyP*) was compared with the growth of the MtbΔ*mbtB* parental strain under identical conditions to determine whether the mutations impacted the ability of the bacteria to acquire iron from heme. For comparisons, all A_{750} measurements were normalized to the A_{750} measured for the MtbΔ*mbtB* parental strain in the presence of mycobactin J at the same time point.

Heme and Protoporphyrin IX (PPIX) Titration into Mt-DyP

Solutions were made, and titration experiments were performed as described previously (21, 22). Heme (23) and PPIX (24) solutions were freshly prepared prior to each experiment. Briefly, ~4 mg of heme was dissolved in 1 ml of ice-cold 100 mM NaOH and vortexed periodically over a 20-min period. One ml of 1 M Tris (pH 7.4) was added to the solution and centrifuged for 10 min at 4 °C at 13,000 rpm. The supernatant was then diluted with 50 mM Tris (pH 7.4) and 150 mM NaCl and centrifuged again at 13,000 rpm for 10 min to remove undissolved heme. Final concentrations were determined using ϵ_{385} of 58.44 mM^{-1} cm^{-1}. Crystals of PPIX were dissolved in 150 mM NaCl, vortexed periodically over 20 min, and centrifuged. Supernatant was collected and diluted in 2.7 N HCl, where the concentration was determined using an ϵ_{408} of 262 mM^{-1} cm^{-1}. PPIX solutions were diluted in 50 mM Tris-HCl (pH 7.4) and 150 mM NaCl for experiments. Heme and PPIX solutions were protected from light and used within 12 h. Micromolar increments of either heme or PPIX were titrated into either 5 or 2.5 μM purified apo-Mt-DyP, respectively, in 50 mM Tris-HCl (pH 7.4) and 150 mM NaCl.

Kinetics of Enzymatic Activity within Mt-Enc

Mt-DyP—All enzymatic reactions were performed in 100-μl reactions. Peroxidase activity utilizing guaiacol as a substrate was monitored over 20 min as a change in absorbance at 470 nm, indicative of the production of tetraguaiacol. 2 μM holo-Mt-DyP (reconstituted with heme to obtain a 1:1 heme/protein molar ratio), apo-Mt-DyP, Mt-Enc, and Mt-Enc·DyP (grown in 0.7 mM δ-ALA, where the heme bound Mt-DyP concentration is estimated from Soret peak intensity utilizing UV-visible spectroscopy) were assayed in the presence of 10 mM H_2O_2 (Sigma-Aldrich) and 10 mM guaiacol (Sigma-Aldrich) (25) in 100 mM sodium citrate at pH 4. Reactions were initiated upon the addition of H_2O_2 and were monitored over a 12-min period, observing the change in absorbance at 470 nm by UV-visible spectrometry (DU-800 spectrophotometer, Beckman-Coulter) at 25 °C. The rate of product formation was calculated using the extinction coefficient of 26,600 M^{-1} cm^{-1} of tetraguaiacol at 470 nm (26).

Further analysis of the activity of Mt-DyP was carried out by utilization of 2,2′-azino-bis(3-ethylbenzothiazoline-6-sulfonic acid (ABTS) as a substrate, as described previously (27). Briefly, 250 μM ABTS was added to a reaction mixture containing 1.25 μM Mt-DyP, Mt-Enc, or Mt-Enc·DyP (grown in 0.7 mM δ-ALA, where the heme-bound Mt-DyP concentration is estimated from Soret peak intensity) in 50 mM HEPES at pH 5.5. The reaction was initiated upon the addition of 10 μM H_2O_2 and monitored for 10 min at 420 nm by UV-visible spectrometry (DU-800 spectrophotometer, Beckman-Coulter) at 25 °C. The rate of product formation was calculated using the extinction coefficient of 36,000 M^{-1} cm^{-1} of the ABTS radical cation at 420 nm (28).

To assess deferrocheletase activity, 5 μg of *Mycobacterium smegmatis* mc^{2}155 cytosol and cell membrane was isolated as described previously (29, 30) and incubated with exogenous, recombinant holo-Mt-DyP (5 μM) at 25 °C. The change at 402 nm was monitored over 10 min by UV-visible spectrometry (DU-800 spectrophotometer, Beckman-Coulter).

Mt-BfrB—Ferroxidase activity was measured following an amended protocol described by Khare *et al.* (31), whereby activity was monitored at 320 nm with some differences. Briefly, purified Mt-BfrB apo-Mt-BfrB, apo-Mt-BfrBΔ167–181, and Mt-Enc·BfrB proteins were dialyzed against 100 mM MES, pH 6.5, and 100 mM KCl. Ferrous ammonium sulfate (FAS) was dissolved in degassed 0.1 M HCl for a 5 mM stock solution of FAS diluted in 100 mM MES, pH 6.5, and 100 mM KCl. FAS was added to a 1 μM concentration of a 24-subunit assembly of Mt-BfrB at 25 °C to a final FAS concentration of 100 μM. Ferrous iron oxidation was monitored by observing the change in absorbance at 320 nm over 10 min, using a DU-800 spectrophotometer (Beckman-Coulter).

Mt-FolB—Mt-FolB aldolase activity was monitored by fluorimetry, as described previously (16). Briefly, Mt-FolB, Mt-Enc·FolB, or Mt-Enc (1 μM) was assayed in the presence of 80 μM 7,8-dihydroneopterin (Sigma-Aldrich) in 50 mM Tris-HCl, pH 8.0, and 150 mM NaCl. The production of 6-hydroxymethyl-7,8-dihydropterin was determined by fluorimetry (Hitachi F-4500 fluorescence spectrometer), where the λ_{ex} was
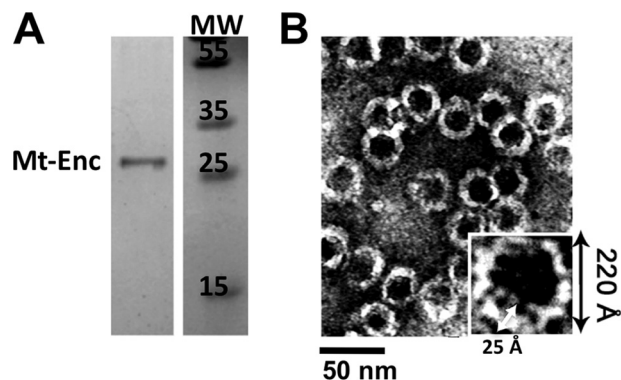
FIGURE 2. **Mt-Enc assembles into a nanoparticle.** *A*, elution fractions of Mt-Enc$_{His}$ purification. *B*, EM image of purified Mt-Enc$_{His}$; the *inset* shows a single particle with a double-sided arrow indicating ~220-Å Mt-Enc particle diameter and thickness of ~25 Å.

430 nm and the change in λ_{em} at 524 nm was monitored. Data were acquired over 35 min.

RESULTS

Mt-Enc Is a Nanocompartment—Mt-Enc is the only Enc homolog in the *M. tuberculosis* proteome. Recombinant Mt-Enc was purified to near homogeneity, as shown by SDS-PAGE (Fig. 2*A*). EM analysis revealed that purified Mt-Enc forms a shell-like nanocompartment with a diameter of ~220 Å and shell thickness of ~25 Å, as determined using ImageJ (32) (Fig. 2*B*). The shell diameter and thickness of Mt-Enc are in good agreement with the previously solved structure of the 60-subunit Tm-Enc nanocompartment (6), suggesting that Mt-Enc also forms a 60-subunit assembly.

Preliminary Characterization of Mt-DyP—The gene that encodes for Mt-Enc is in a two-gene operon with Mt-DyP. Mt-DyP is a previously uncharacterized protein; therefore, we first determined the function of Mt-DyP. Two DyP-like peroxidases from *E. coli*, Ec-YfeX and Ec-EfeB, were proposed to extract iron from heme while keeping the tetrapyrrole ring intact (11). This hypothesis was based on PPIX accumulation upon overexpression of Ec-YfeX in *E. coli* (11). However, another study reported that Ec-YfeX is a typical heme-dependent dye-decolorizing peroxidase and does not possess deferrocheletase activity (12). Recently, *Rhodococcus jostii* DypB (Rj-DypB) found in an operon with Enc (Rj-Enc), was shown to be a heme-dependent dye-decolorizing peroxidase with lignin-degrading capabilities (27). Mt-DyP is 57% (over 343 amino acids) and 28% (over 152 amino acids) sequence-identical to Rj-DypB (DyP Class B) and Ec-YfeX (DyP Class A), respectively.

Mt-DyP was purified to homogeneity by nickel affinity chromatography (Fig. 3*A*). Purified Mt-DyP was colored pink, suggesting heme-bound Mt-DyP. Size exclusion chromatography was utilized to separate apo- and heme-bound species, where three distinct oligomeric states of Mt-DyP were separated and analyzed by UV-visible spectroscopy at 402 nm to determine heme-bound fractions (Fig. 3, *C* and *D*). Monomeric Mt-DyP was in its apo-form, similar to other bacterial DyPs (DyP2 from *Amycolatopsis* sp. 75iv2 and *E. coli* apo-EfeB (33, 34)), and a minor dimeric Mt-DyP species with a substoichiometric quantity of heme was also observed. Tetrameric Mt-DyP had a nearly 1:1 molar stoichiometry of heme bound. Finally, Mt-DyP
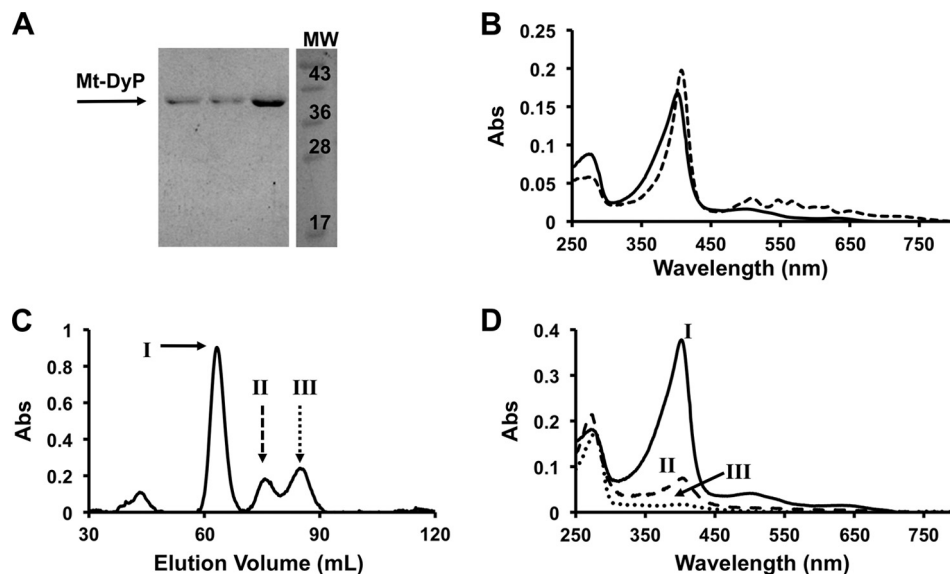
FIGURE 3. **Preliminary characterization of Mt-DyP.** *A*, elution fractions from nickel affinity purification of Mt-DyP. *B*, UV-visible spectra of heme-bound (*solid line*) or PPIX-bound (*dashed line*) Mt-DyP to a 1:1 molar ratio. *C*, representation of three distinct elution peaks from a gel filtration experiment performed on an S200 16/600 Superdex column, yielding an Mt-DyP tetramer (*I*, 116 kDa), dimer (*II*, 58 kDa), and a monomer (*III*, 29 kDa), where their respective molecular weights were calculated using molecular weight standards (Bio-Rad). *D*, UV-visible spectra of elutions resulting from three elution peaks post-gel filtration from *C*, demonstrating heme content at ~400 nm. The tetramer (*solid line*) has 1:1 heme/protein molar ratio; dimer (*dashed line*) has trace amounts of heme, whereas the monomer is in its apo-form (*dotted line*).

bound both heme and PPIX (Fig. 3*B*). Titration of apo-Mt-DyP with heme suggests a 1:1 molar stoichiometry, similar to the titration of Mt-DyP with PPIX, which also implies a 1:1 molar stoichiometry (data not shown).

To determine whether Mt-DyP possesses heme peroxidase activity, we tested the ability of tetrameric holo-Mt-DyP to form compound I, the heme-dependent peroxidase intermediate. The irreversible reaction of a heme-dependent peroxidase with H_2O_2 results in the formation of compound I, an oxidized form of heme, where Fe(III) is oxidized to Fe(IV)=O along with the formation of a porphyrin π-cation radical; compound I is then poised to oxidize its substrate. Upon the addition of H_2O_2 to holo-Mt-DyP, a color change of brown to green occurs, which is indicative of compound I formation. Further, the UV-visible spectrum of holo-Mt-DyP after the addition of H_2O_2 at pH 7.4 displayed a decrease and blue-shifted, hypochromatic Soret peak from 402 to 398 nm, with the emergence of a slight shoulder at around 345 nm (Fig. 4*A*) and a broad hyperchromaticity between 576 and 648 nm (Fig. 4*A*, *inset*) similar to that observed for Rj-DypB (35) and horseradish peroxidase compound I intermediates (36) (Table 1). These results show that holo-Mt-DyP forms compound I in the presence of H_2O_2, indicating that Mt-DyP is a heme peroxidase.

Mt-DyP was tested for peroxidase activity using either guaiacol or ABTS as substrates. First, peroxidase activities of holo- and apo-Mt-DyP were compared utilizing guaiacol as a substrate (Fig. 4*B*). Apo-Mt-DyP had no detectable peroxidase activity compared with holo-Mt-DyP, suggesting that Mt-DyP is a heme peroxidase that can utilize guaiacol as a substrate. The specific activity of Mt-DyP forming tetraguaiacol under the conditions tested was 0.041 ± 0.004 μmol min^{-1} mg^{-1}, and the k_{cat} is 1.46 ± 0.15 min^{-1}. Mt-DyP has a 50-fold lower k_{cat} value than a DyP from a white rot fungus *Phanerochaete chrysosporium* (37); however, it has been noted that *M. tuberculosis*
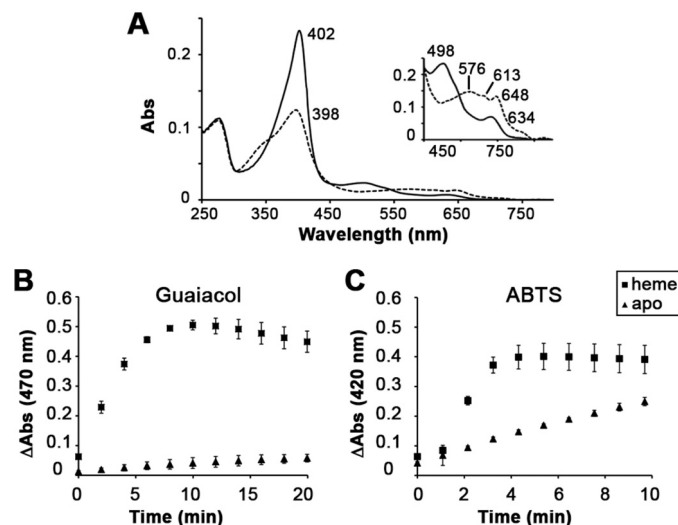

FIGURE 4. **Peroxidase activity of Mt-DyP.** *A*, absorbance spectrum of holo-Mt-DyP (~2.5 μM) in the absence (*solid line*) and presence (*dashed line*) of 100 μM H_2O_2, where in the presence of H_2O_2, the formation of Compound I is observed, indicative of a heme-dependent peroxidase. *Inset*, the visible region magnified 10-fold. *B*, holo-Mt-DyP (2 μM) peroxidase activity utilizing guaiacol (10 mM) as a substrate in the presence of H_2O_2 (10 mM) at pH 4.0 was monitored by observing the production of tetraguaiacol at 470 nm. *C*, holo-Mt-DyP (1.25 μM) peroxidase activity utilizing ABTS (250 μM) as a substrate in the presence of H_2O_2 (10 μM) at pH 5.5 was monitored by observing the change in absorbance at 420 nm.

enzymes may have slower rates of reactions compared with their homologs (38, 39). Second, utilizing ABTS as the reducing substrate, holo-Mt-DyP produced an ABTS radical cation in the presence of H_2O_2 indicative of an active peroxidase, whereas apo-Mt-DyP displayed background activity (Fig. 4*C*). The specific activity of Mt-DyP producing ABTS radical cation under the conditions tested was 0.052 ± 0.005 μmol min^{-1} mg^{-1}, and the k_{cat} is 2.11 ± 0.25 min^{-1}. Mt-DyP has a 50-fold lower k_{cat} value than Rj-DypB (40). These results suggest that Mt-DyP is a heme peroxidase.

TABLE 1
Absorption spectral comparisons of resting and compound I forms of heme-dependent peroxidases

Name	Resting	Compound I	Source/Reference
	nm	*nm*	
Mt-DyP	402, 498, 634	398, 576, 613, 648	This study
Rj-DypB	404, 503, 634	400, 580, 613, 648	Ref. 35
HRP	403, 498, 640	400, 525 (sh), 577, 622 (sh), 651	Ref. 36

Although Mt-DyP has heme-dependent peroxidase activity, Mt-DyP deferrochelatase activity was also tested because we have shown that Mt-DyP can bind PPIX (Fig. 3*B*). Heme-bound Mt-DyP was incubated with either *M. smegmatis* mc²155 cytosolic or membrane fractions, as described previously for Ec-YfeX (11). The reaction was followed by UV-visible spectroscopy, and no significant change in the Soret region was observed under the conditions tested, indicating that no PPIX product was formed as a result of iron extraction from heme (Fig. 5*A*). These results suggest that Mt-DyP does not possess deferrochelatase activity *in vitro*. However, deferrochelatase activity requires an electron source for iron extraction from heme, and the *in vitro* conditions tested may not contain the necessary components. Thus, we sought to investigate the function of Mt-DyP *in vivo* by observing the effects of Mt-DyP upon mycobacterial heme iron acquisition.

Mycobacteria possess a heme uptake pathway (20, 41) along with a cytosolic heme-degrading enzyme, MhuD, which has been shown to degrade heme by cleavage of the tetrapyrrole ring to release iron and mycobilins as products (42, 43). To test for Mt-DyP deferrochelatase activity, we utilized a mycobactin-deficient *M. tuberculosis* strain, MtbΔ*mbtB*, which has an interrupted mycobactin biosynthetic pathway to prevent siderophore-mediated iron acquisition (20, 41) and cannot utilize Fe(III) in the absence of exogenous siderophore (mycobactin). Thus, MtbΔ*mbtB* may only sequester iron via the heme uptake pathway. We assessed growth of MtbΔ*mbtB* mutants lacking MhuD and/or Mt-DyP against MtbΔ*mbt*B alone in limiting heme concentrations (Fig. 5*B*). MtbΔ*mbtB* supplemented with 0.2 μM heme grows to ~60% of the growth achieved in the presence of exogenous siderophore (mycobactin). The MtbΔ*mbtB*Δ*dyP* mutant grew at a similar rate to MtbΔ*mbtB* in the presence of 0.2 μM heme. In contrast, the growth rate of MtbΔ*mbtB*Δ*mhuD* was significantly attenuated in the presence of 0.2 μM heme compared with MtbΔ*mbtB* (20% *versus* 60%) (Fig. 5*B*). These results suggest that MhuD, but not Mt-DyP, is required for heme degradation when heme is the sole iron source, at least when MhuD is present. To determine whether Mt-DyP is required for iron sequestration in the absence of MhuD, we generated the triple mutant, MtbΔ*mbtB*Δ*mhuD*Δ*dyP*. Growth of MtbΔ*mbtB*Δ*mhuD*Δ*dyP* in the presence of 0.2 μM heme was significantly attenuated compared with MtbΔ*mbtB* (18% *versus* 60%) but no more so than MtbΔ*mbtB*Δ*mhuD*, indicating that Mt-DyP is not required for iron sequestration from heme in either the presence or absence of MhuD. Taken together, these results indicate that under the conditions tested, Mt-DyP probably does not possess deferrochelatase activity.

Co-purification of Mt-Enc and Cargo Proteins—Mt-DyP is found upstream of Mt-Enc and harbors a C-terminal extension, similar to that observed in other organisms that also contain
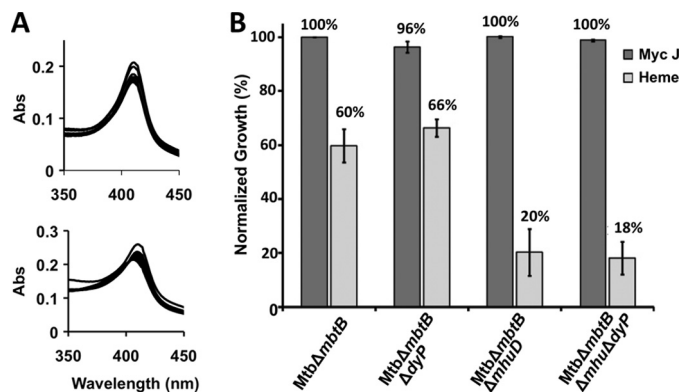

FIGURE 5. **Mt-DyP demonstrates no deferrochelatase activity.** *A*, *M. smegmatis* mc²155 cytosolic fraction (5 μg) (*top*) and *M. smegmatis* mc²155 Triton X-114-extracted membrane (5 μg) (*bottom*) were incubated with holo-Mt-DyP (5 μg). Possible deferrochelatase activity was monitored over 20 min, where a decrease in Soret intensity (~410 nm) would be observed over time. *B*, MtbΔ*mbtB*, MtbΔ*mbtB*Δ*dyP*, MtbΔ*mbtB*Δ*mhuD*, and MtbΔ*mbtB*Δ*mhuD*Δ*dyP* were grown in 7H9-OADC containing 0.01% tyloxapol medium supplemented with either 0.2 μM heme or mycobactin J (*Myc J*) (10 ng/ml). Growth was monitored by measuring absorbance at 750 nm, and the results shown were taken at 18–20 days, when all strains in the presence of mycobactin J plateaued. The results shown are A_{750} measurements normalized to the growth of the MtbΔ*mbtB* in the presence of mycobactin J at the same time point and are the mean ± S.E. (*error bars*) of two independent experiments.

Enc and DyP in a two-gene operon. Thus, we propose that Mt-DyP interacts with Mt-Enc (6, 27). The two-gene operon, whose gene products are Mt-Enc and Mt-DyP, was cloned into an expression vector so that Mt-Enc has a C-terminal His tag and Mt-DyP does not. Purification of overexpressed Mt-DyP and Mt-Enc by affinity chromatography demonstrated that Mt-DyP and Mt-Enc co-elute (Fig. 6*A*), suggesting that an Mt-Enc·DyP protein complex has formed. EM analysis was utilized to visualize the Mt-Enc·DyP complex, revealing a large sphere similar to Mt-Enc (Fig. 2*B*) containing a density that we presume to be Mt-DyP (Fig. 6*A*) because no discernable density was observed within Mt-Enc alone (Fig. 2*B*). The diameter of the Mt-Enc nanocompartment is ~220 Å, and its cargo, Mt-DyP, has a diameter ranging from 70 to 90 Å, as measured by ImageJ (32). The oligomeric state of encapsulated Mt-DyP is unknown. To test whether the C-terminal extension of Mt-DyP is required to target Mt-DyP to be encapsulated by Mt-Enc, we deleted the last 24 C-terminal amino acids of Mt-DyP (Mt-DyPΔ312–335). Mt-Enc and Mt-DyPΔ312–335 were then coexpressed, and upon purification, Mt-DyPΔ312–335 was observed in the flow-through, and only Mt-Enc was eluted, as seen by SDS-PAGE (Fig. 6*D*). These results suggest that Mt-Enc encapsulates Mt-DyP via its C-terminal tail.

We previously carried out studies of Mt-BfrB (ferritin (44)) and Mt-FolB (second enzyme in folate biosynthesis (16)) and noted that both mycobacterial proteins have extra ~20-amino acid C-terminal extensions (Fig. 1) in comparison with most of
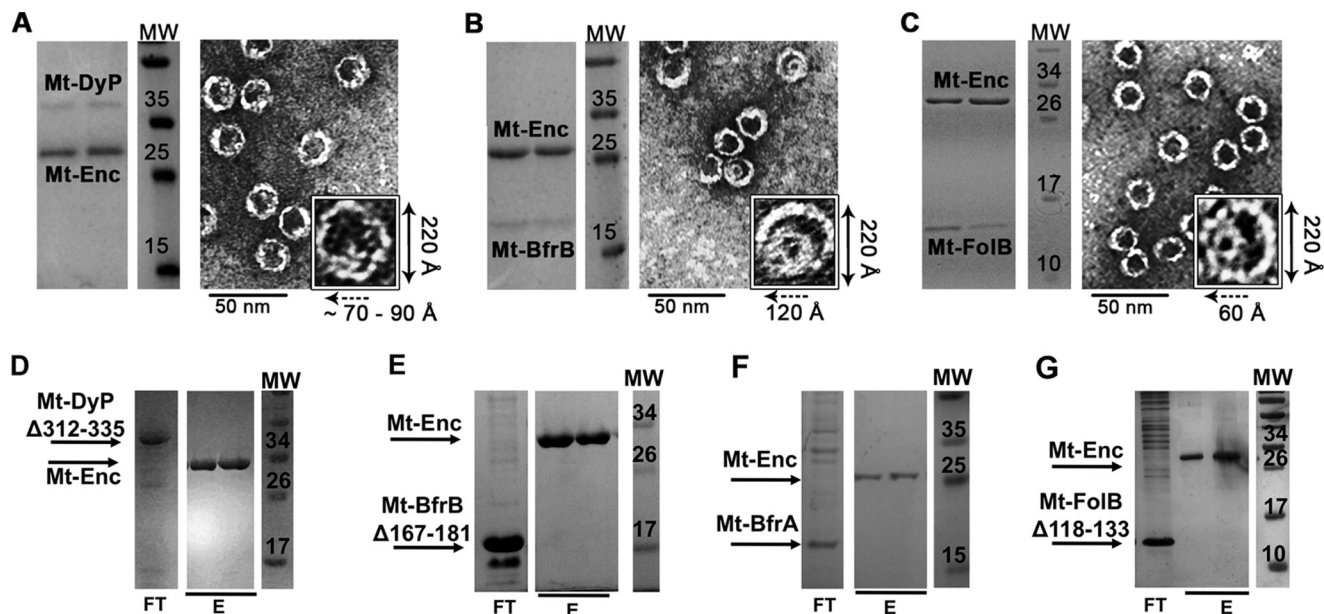
FIGURE 6. **Characterization of Mt-Enc with cargo proteins.** Mt-Enc and co-elution of putative interacting *M. tuberculosis* protein: Mt-DyP (~37 kDa) (*A*); Mt-BfrB (~20 kDa) (*B*); or Mt-FolB (~14 kDa) (*C*). *Left*, SDS-PAGE of eluted fractions with a molecular weight marker (*MW*). *Right*, EM images with an *inset* of a single magnified Mt-Enc particle with cargo protein with a *double-sided arrow* indicating 220-Å Mt-Enc particle diameter. *Dashed arrow*, diameter of cargo protein. *D–G* demonstrate that proteins lacking a C-terminal extension do not co-purify with Mt-Enc. Mt-Enc does not co-elute with Mt-DyPΔ312–335 (*D*), Mt-BfrBΔ167–181 (*E*), Mt-BfrA (*F*), or Mt-FolBΔ118–133 (*G*). Shown are flow-through (*FT*) and elution (*E*) fractions analyzed by SDS-PAGE.

their other bacterial homologs. Both Mt-BfrB (13) and Mt-FolB (16) are known to have antioxidant properties, along with DyPs (45, 46). Due to the observation that ferritin-like proteins with C-terminal extensions are contained within operons with Enc and are proposed to interact (6), we hypothesized that Mt-BfrB and Mt-FolB may also interact with Mt-Enc through their C-terminal extensions.

Mt-Enc encapsulates fully assembled Mt-BfrB, where Mt-BfrB forms a 24-subunit icosahedral shell (44), in contrast to Mt-Enc, which forms a 60-subunit icosahedral shell. We coexpressed Mt-Enc with a C-terminal His tag together with full-length Mt-BfrB. Mt-Enc and Mt-BfrB co-eluted from an affinity column (Fig. 6*B*). Visualization of the Mt-Enc·BfrB complex by EM clearly shows a smaller spherical shell within the interior of a larger shell. The larger shell has a diameter of ~220 Å, similar to Mt-Enc alone, and the inner shell has a diameter of ~120 Å, similar to that of Mt-BfrB (Fig. 6*B*) (44), suggesting that Mt-Enc encapsulates fully assembled 24-subunit Mt-BfrB (Fig. 6*B*). Because it is proposed that Mt-Enc encapsulates its target protein via a C-terminal extension, Mt-BfrB was truncated to remove 15 C-terminal residues (Mt-BfrBΔ167–181). First, we showed by analytical gel filtration analysis that Mt-BfrBΔ167–181 has an elution profile similar to that of Mt-BfrB, suggesting that it retains its 24-subunit assembly in the absence of its C-terminal extension (data not shown). Second, upon coexpression of Mt-Enc and Mt-BfrBΔ167–181 followed by affinity chromatography purification, Mt-BfrBΔ167–181 was observed in the flow-through and did not co-elute with Mt-Enc (Fig. 6*E*). The other *M. tuberculosis* ferritin homolog, Mt-BfrA, also self-assembles into a 24-subunit nanocage (38, 39); however, Mt-BfrA does not possess a C-terminal extension. When Mt-BfrA was coexpressed with Mt-Enc followed by affinity chromatography purification, it did not co-elute with Mt-Enc (Fig. 6*F*).

These observations validate the importance of the C-terminal extension in potentiating Mt-BfrB binding to the interior of the Mt-Enc compartment.

Similarly, Mt-FolB contains an extended C terminus composed of aliphatic amino acids (Fig. 1); thus, it is possible that Mt-FolB might interact with Mt-Enc via its C-terminal tail. Coexpression of Mt-FolB and Mt-Enc resulted in co-purification of Mt-FolB with Mt-Enc. EM images of the Mt-Enc·FolB complex showed fully assembled Mt-Enc that contained a potential protein cargo (Fig. 6*C*). The diameter of the cargo is ~60 Å, similar to the diameter of either the tetrameric or octameric forms of Mt-FolB (16), suggesting that Mt-Enc also encapsulates Mt-FolB. Upon deletion of the C-terminal tail of Mt-FolB, where Mt-FolBΔ118–133 retains its enzyme activity (16), coexpression with Mt-Enc followed by purification resulted in the elution of Mt-Enc alone (Fig. 6*G*). These results suggest that Mt-FolB can be encapsulated by Mt-Enc via its C-terminal extension.

EM images show that nearly all Mt-Enc nanocompartments are occupied by Mt-DyP (~80%), which was coexpressed from a single plasmid. Fewer Mt-Enc assemblies were occupied with Mt-BfrB or Mt-FolB (<30%); however, Mt-Enc and Mt-BfrB or Mt-FolB were coexpressed from separate plasmids. Reduced encapsulation is not surprising because heterologous overexpression of mycobacterial proteins in *E. coli* is not representative of the coupled translation or tight regulation in *M. tuberculosis*.

Analysis of Enzymatic Activity of Cargo Proteins within Mt-Enc—We have demonstrated that Mt-DyP has heme-dependent peroxidase activity that may utilize guaiacol or ABTS as substrates. Previously, it has been shown that Mt-BfrB has ferroxidase activity (31), and Mt-FolB has aldolase activity even in its C-terminal truncated form (16). Furthermore, we have shown that coexpression of each of these proteins with Mt-Enc
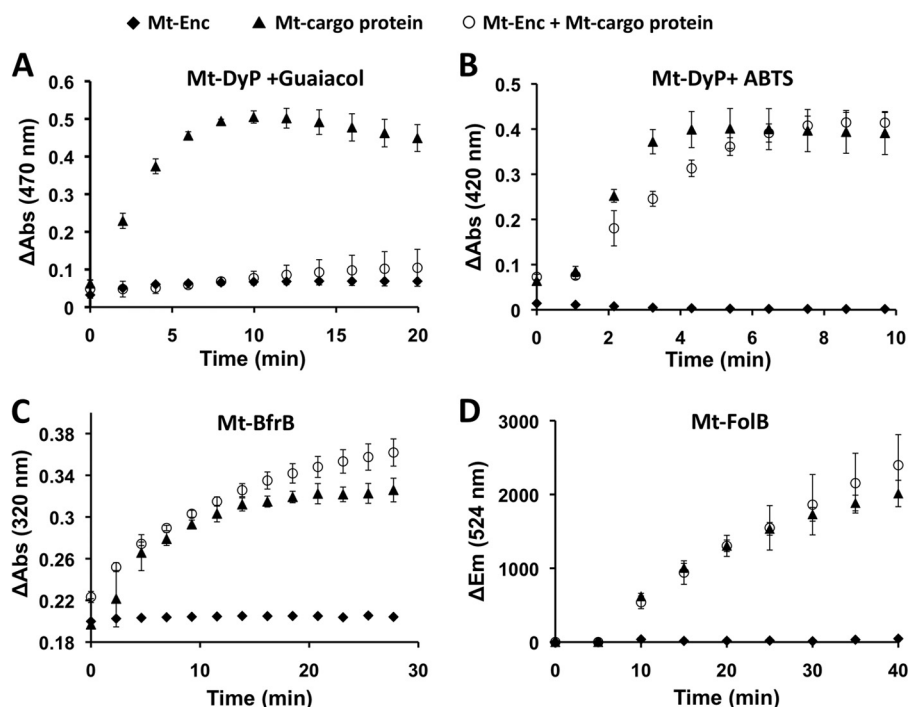
FIGURE 7. **Analysis of enzymatic activity of cargo protein within Mt-Enc.** *A*, Mt-DyP peroxidase activity utilizing guaiacol as a substrate in the presence of H_2O_2 was monitored by observing the production of tetraguaiacol at 470 nm. *B*, Mt-DyP peroxidase activity utilizing ABTS as a substrate in the presence of H_2O_2 was monitored by observing the change in absorbance at 420 nm. *C*, Mt-BfrB ferroxidase activity was monitored by observing the oxidation of ferrous iron to ferric iron at 320 nm. The encapsulated BfrB was compared with the rate of the Mt-BfrBΔ167–181. *D*, Mt-FolB enzyme activity was monitored, utilizing 7,8-dihydroneopterin as a substrate, by observing the change in emission at 524 nm. *Error bars*, S.E.

results in encapsulation of each cargo protein via its C-terminal extension (Fig. 6). Next, we examined whether Mt-DyP, Mt-BfrB, and Mt-FolB retain their activities when encapsulated by Mt-Enc.

Mt-DyP—To ensure that C-terminal truncation of Mt-DyP did not result in loss of activity, we demonstrated that heme-bound Mt-DyPΔ312–335 retained its peroxidase activity with both guaiacol and ABTS as substrates (data not shown). In an attempt to produce encapsulated holo-Mt-DyP, Mt-Enc and Mt-DyP were coexpressed in the presence of δ-ALA. After purification of the Mt-Enc·DyP complex, the heme concentration within the complex (and presumably bound to Mt-DyP) was quantified using UV-visible spectroscopy (to determine heme concentration) and SDS-polyacrylamide gel band intensity analysis (to determine Mt-DyP concentration) using ImageJ (32). Utilizing either guaiacol or ABTS as substrates in the presence of H_2O_2, we assessed the peroxidase activity of holo-Mt-DyP within Mt-Enc. With guaiacol as a substrate, Mt-Enc·DyP showed minimal peroxidase activity compared with unencapsulated holo-Mt-DyP (Fig. 7A). In contrast, encapsulated Mt-DyP retained peroxidase activity with ABTS as a substrate similar to unencapsulated holo-Mt-DyP (Fig. 7B), although we observed a slightly decreased rate. Within Mt-Enc, we could not monitor the oligomeric state of holo-Mt-DyP, and we showed above that holo-Mt-DyP was active as a tetramer (Fig. 3, *C* and *D*); thus, the observed decrease in rate of activity of encapsulated Mt-DyP may be due to the presence of various heme-bound Mt-DyP oligomeric states. In light of these results, we have demonstrated that Mt-DyP retains heme peroxidase activity while encapsulated; however, it appears to have a more limited substrate set than unencapsulated holo-Mt-DyP.

Mt-BfrB—To determine the activity of encapsulated Mt-BfrB, ferroxidase activity of the Mt-Enc·BfrB complex was measured at 320 nm to monitor iron core formation (47). To determine if the Mt-Enc·BfrB complex maintained ferroxidase activity, we quantified the amount of encapsulated Mt-BfrB by densitometry measurements of SDS-polyacrylamide gel bands using ImageJ (32). Upon the addition of ferrous iron to Mt-BfrB alone, we observed ferroxidase activity. The specific activity of Mt-BfrB oxidizing Fe(II) is 0.073 ± 0.006 μmol min^{-1} mg^{-1}, where the activity is similar to a previous study of Mt-BfrB (31). Truncation of the C-terminal tail of Mt-BfrB, Mt-BfrBΔ167–181, resulted in fully assembled ferritin (data not shown) with a slightly reduced oxidation rate of Fe(II) (data not shown), as also observed by Khare *et al.* (31). In contrast, Mt-Enc alone was not capable of oxidizing Fe(II) (Fig. 7C). Mt-BfrB encapsulated in Mt-Enc retained its ferroxidase activity with a rate similar to that of Mt-BfrBΔ167–181 (Fig. 7C). Reduction in the rate of Fe(II) oxidation by encapsulated Mt-BfrB similar to that of Mt-BfrBΔ167–181 suggests that the C-terminal tail of Mt-BfrB is probably involved in binding to the interior of Mt-Enc, rendering it unavailable to enhance ferroxidase activity to the level observed for unencapsulated full-length Mt-BfrB.

Mt-FolB—Aldolase activity of Mt-FolB within Mt-Enc was assayed by measuring the production of 6-hydroxymethyl-7,8-dihydropterin as a change in fluorescence emission at 524 nm. The concentration of encapsulated Mt-FolB was estimated by densitometry measurements from SDS-PAGE analysis using ImageJ (32). The level of aldolase activity achieved upon the addition of a 1.5-fold molar excess of encapsulated Mt-FolB was similar to that of unencapsulated Mt-FolB (Fig. 7D). The specific activity of Mt-FolB is 0.18 ± 0.02 μmol min^{-1} mg^{-1}, sim-

ilar to our previous study of Mt-FolB (31). Mt-Enc alone did not exhibit aldolase activity. These results suggest that Mt-FolB retains aldolase activity while encapsulated.

DISCUSSION

Encapsulins are a recently discovered family of conserved prokaryotic proteinaceous nanocompartments, first described by Sutter *et al.* (6). Enc cargo proteins have C-terminal tails required for their encapsulation, where Enc and cargo proteins are usually found in a two-gene operon, suggesting tight translational coupling. We have demonstrated that *M. tuberculosis* has an Enc nanocompartment similar in diameter to that of Tm-Enc (6), implying that it is also a 60-subunit icosahedral shell. Mt-Enc exists in a two-gene operon, where the upstream Mt-DyP harbors a C-terminal extension. Coexpression of Mt-DyP and Mt-Enc results in encapsulation of Mt-DyP by Mt-Enc, an interaction mediated by the C-terminal tail of Mt-DyP. Although it is possible that Mt-Enc and Mt-DyP are expressed as a polycistronic mRNA transcript, the transcriptional and translational regulation of these proteins in *M. tuberculosis* is unknown. Additionally, we have demonstrated that Mt-BfrB and Mt-FolB are also encapsulated by Mt-Enc, via an interaction mediated by the C-terminal extension of each protein cargo, where loss of this C-terminal tail abolishes the interaction with Mt-Enc and their subsequent encapsulation. These results show that Mt-Enc could potentially compartmentalize other mycobacterial enzymes that bear a C-terminal tail.

Compartmentalization is important for organization, increasing the local concentration of functionally related enzymes and confining unstable reaction intermediates within the cell. Many bacteria produce protein-based microcompartments (MCPs) that are larger than encapsulin nanocages but also encapsulate various cargo enzymes (48, 49). In *Salmonella enterica*, MCPs are proposed to organize reactions as well as isolate "unstable" reaction intermediates that may form within the compartment (48), such as proteins involved in 1,2-propanediol utilization (Pdu) (50) and ethanolamine utilization (Eut) (48). Indeed, a recent comparative genomics study predicts that in some organisms, MCPs may encapsulate bacterioferritin (51), similar to Mt-Enc. A common feature of MCP-compartmentalized enzymes is an additional short N-terminal sequence found to be necessary for targeting enzymes to the MCP interior (48, 52), akin to the cargo protein C-terminal extensions required for their encapsulation in Enc (6). It could be surmised that engineering a C-terminal tail on an enzyme could potentiate encapsulation by Mt-Enc and possibly deliver and/or release cargo enzymes under conditions where the compartment disassembles.

This study and previous ones (6, 27) demonstrate that encapsulins from four different organisms self-assemble into 60-subunit nanocompartments with a diameter of ~220–240 Å and can accommodate multiple copies of a single cargo protein. Distant sequence homologs of Tm-Enc, *Pyrocuccus furiosus* PfV, and the major caspid protein gp5 of the HK97 virus (18 and 9% sequence identity, respectively) are close structural homologs of Tm-Enc (root mean square deviations of 2.39 and 2.65 Å, respectively) (53). All three proteins form icosahedral cages; however, Tm-Enc has $T = 1$ symmetry with 60 subunits/cage (6), PfV has $T = 3$ symmetry with 180 subunits/cage (53),

and gp5 has $T = 7$ symmetry with 420 subunits/cage (54). Thus, one can postulate that Enc homologs, such as Mt-Enc, may form higher symmetry icosahedral cages *in vivo* to allow for more than one cargo protein or even an entire reaction pathway to be encapsulated, as observed for MCPs (49).

Passage of substrates through encapsulin is currently unknown. Charged pores observed for Tm-Enc may mediate substrate specificity (6), regulating the flux of substrates in and out of encapsulin that are available to the protein cargo. This may also be the case with Mt-Enc and the differential activity of encapsulated Mt-DyP with various electron-donor substrates, where guaiacol is neutral and ABTS is negatively charged. Rhamanpour and Bugg (27) reported peroxidase activity of Rj-DypB when encapsulated within Rj-Enc with lignin as a substrate. This was an unexpected result because the expected pore size of Enc (<5 Å wide) is not large enough to accommodate the passage of lignin (27), suggesting that the Enc pore is dynamic. Indeed, utilizing dynamic light scattering, it was observed that native Rj-Enc has a diameter of 220 Å; however, after acidic disassembly followed by reassembly with Rj-DyP, the complex has a diameter of 310 Å (27). The flexibility of the Enc monomer may allow Enc to form compartments consisting of more than 60 subunits or to expand its pore size to modulate substrate entry (6, 27).

Mycobacteria are resistant to assault by host oxidative metabolites (46), where the presence of iron storage proteins and peroxidases aids in mycobacterial viability. A recent study demonstrated that an *M. tuberculosis* double deletion mutant of *bfrA* and *bfrB* exhibited vulnerability to oxidative stress (14), and the MtbΔ*bfrB* mutant has greater susceptibility than the MtbΔ*bfrA* mutant (13, 14), highlighting the importance of Mt-BfrB in *M. tuberculosis* survival during oxidative assault. Mt-BfrB has antioxidant properties by storing iron, thereby preventing the generation of hydroxyl radicals upon oxygen exposure. Furthermore, *in vivo*, it has been shown that Mt-BfrB is up-regulated under hypoxic conditions (55), during assault by NO donors (56), and during adaptation to the stationary phase (57). We have demonstrated that Mt-DyP can function as a heme-dependent peroxidase; thus, Mt-DyP may aid in mycobacteria resistance to host oxidative assault (46). This could potentially hold true for Mt-FolB. Mt-FolB is a 7,8-dihydroneopterin aldolase that is involved in folate biosynthesis, converting folate precursor 7,8-dihydroneopterin to 6-hydroxymethyl-7,8-dihydropterin. Mt-FolB displays cooperative dependence on 7,8-dihydroneopterin binding from an apotetrameric form to active substrate-bound octameric form (16). Furthermore, its substrate possesses antioxidant properties (15, 17). Thus, if *M. tuberculosis* encounters host oxidative stress, then 7,8-dihydroneopterin may function as an antioxidant maintaining a relatively low cellular concentration. However, when oxidative stress diminishes, the concentration of 7,8-dihydroneopterin would increase to the critical level to form active, octameric Mt-FolB, and *M. tuberculosis* would continue with its normal folate biosynthetic pathway (16). Recently, an *in vitro* study showed that there were five Mt-FolB reaction products (58). Another potential benefit of encapsulation of Mt-FolB could be to (*a*) prevent side products of the reaction forming and (*b*) allow 7,8-dihydroneopterin to remain "free" within

the cytosol to act as an antioxidant. Thus, *M. tuberculosis* encapsulation of proteins may provide the bacterium multiple mechanisms for protecting itself from oxidative damage arising from host immune defenses.

Encapsulation of DyP and ferritin homologs has previously been observed in other organisms (6, 27); however, there is no evidence that Enc interacts with FolB in other organisms. A recent study suggests that a potential *Haliangium ochraceum* aldolase is compartmentalized by a bacterial BMC by its C-terminal extension (Fig. 1*A*) (59). Furthermore, *M. tuberculosis* i*n vivo* microarray data suggest that Mt-Enc and Mt-FolB both are up-regulated under hypoxic conditions (60) and exposure to cephalexin (61), further suggesting that they indeed may interact.

This study provides the first evidence of a mycobacterial nanocompartment that has the ability to encapsulate cargo proteins, where encapsulated cargo proteins retain their enzymatic activities. To date, there are no reports illustrating the formation of a proteinaceous nanocompartment in mycobacteria. It is unknown which cargo protein(s) Mt-Enc encapsulates *in vivo*, how it is regulated, and whether it can accommodate multiple cargo proteins. As has been suggested for other bacterial compartments (62), the potential for carrying cargo and apparent protein stability make Mt-Enc an appealing vehicle to be exploited as a drug delivery system.

REFERENCES

1. World Health Organization (2012) *Global Tuberculosis Report 2012*, World Health Organization, Geneva
2. Tetta, C., Ghigo, E., Silengo, L., Deregibus, M. C., and Camussi, G. (2013) Extracellular vesicles as an emerging mechanism of cell-to-cell communication. *Endocrine* **44,** 11–19
3. Ohno, S., Ishikawa, A., and Kuroda, M. (2013) Roles of exosomes and microvesicles in disease pathogenesis. *Adv. Drug Deliv. Rev.* **65,** 398–401
4. Giri, P. K., Kruh, N. A., Dobos, K. M., and Schorey, J. S. (2010) Proteomic analysis identifies highly antigenic proteins in exosomes from *M. tuberculosis*-infected and culture filtrate protein-treated macrophages. *Proteomics* **10,** 3190–3202
5. Rosenkrands, I., Rasmussen, P. B., Carnio, M., Jacobsen, S., Theisen, M., and Andersen, P. (1998) Identification and characterization of a 29-kilodalton protein from *Mycobacterium tuberculosis* culture filtrate recognized by mouse memory effector cells. *Infect. Immun.* **66,** 2728–2735
6. Sutter, M., Boehringer, D., Gutmann, S., Günther, S., Prangishvili, D., Loessner, M. J., Stetter, K. O., Weber-Ban, E., and Ban, N. (2008) Structural basis of enzyme encapsulation into a bacterial nanocompartment. *Nat. Struct. Mol. Biol.* **15,** 939–947
7. Chiancone, E., Ceci, P., Ilari, A., Ribacchi, F., and Stefanini, S. (2004) Iron and proteins for iron storage and detoxification. *Biometals* **17,** 197–202
8. Kaur, A., Van, P. T., Busch, C. R., Robinson, C. K., Pan, M., Pang, W. L., Reiss, D. J., DiRuggiero, J., and Baliga, N. S. (2010) Coordination of frontline defense mechanisms under severe oxidative stress. *Mol. Syst. Biol.* **6,** 393
9. Kim, S. J., and Shoda, M. (1999) Purification and characterization of a novel peroxidase from *Geotrichum candidum* dec 1 involved in decolorization of dyes. *Appl. Environ. Microbiol.* **65,** 1029–1035
10. Ahmad, M., Roberts, J. N., Hardiman, E. M., Singh, R., Eltis, L. D., and Bugg, T. D. (2011) Identification of DypB from *Rhodococcus jostii* RHA1 as a lignin peroxidase. *Biochemistry* **50,** 5096–5107
11. Létoffé, S., Heuck, G., Delepelaire, P., Lange, N., and Wandersman, C. (2009) Bacteria capture iron from heme by keeping tetrapyrrol skeleton intact. *Proc. Natl. Acad. Sci. U.S.A.* **106,** 11719–11724
12. Dailey, H. A., Septer, A. N., Daugherty, L., Thames, D., Gerdes, S., Stabb, E. V., Dunn, A. K., Dailey, T. A., and Phillips, J. D. (2011) The *Escherichia coli* protein YfeX functions as a porphyrinogen oxidase, not a heme dechelatase. *MBio* **2,** e00248–00211
13. Pandey, R., and Rodriguez, G. M. (2012) A ferritin mutant of *Mycobacterium tuberculosis* is highly susceptible to killing by antibiotics and is unable to establish a chronic infection in mice. *Infect Immun.* **80,** 3650–3659
14. Reddy, P. V., Puri, R. V., Khera, A., and Tyagi, A. K. (2012) Iron storage proteins are essential for the survival and pathogenesis of *Mycobacterium tuberculosis* in THP-1 macrophages and the guinea pig model of infection. *J. Bacteriol.* **194,** 567–575
15. Dántola, M. L., Vignoni, M., Capparelli, A. L., Lorente, C., and Thomas, A. H. (2008) Stability of 7,8-dihydropterins in air-equilibrated aqueous solutions. *Helv. Chim. Acta* **91,** 411–425
16. Goulding, C. W., Apostol, M. I., Sawaya, M. R., Phillips, M., Parseghian, A., and Eisenberg, D. (2005) Regulation by oligomerization in a mycobacterial folate biosynthetic enzyme. *J. Mol. Biol.* **349,** 61–72
17. Schobersberger, W., Hoffmann, G., Hobisch-Hagen, P., Bock, G., Volkl, H., Baier-Bitterlich, G., Wirleitner, B., Wachter, H., and Fuchs, D. (1996) Neopterin and 7,8-dihydroneopterin induce apoptosis in the rat alveolar epithelial cell line L2. *FEBS Lett.* **397,** 263–268
18. Lowry, O. H., Rosebrough, N. J., Farr, A. L., and Randall, R. J. (1951) Protein measurement with the Folin phenol reagent. *J. Biol. Chem.* **193,** 265–275
19. Bradford, M. M. (1976) A rapid and sensitive method for the quantitation of microgram quantities of protein utilizing the principle of protein-dye binding. *Anal. Biochem.* **72,** 248–254
20. Tullius, M. V., Harmston, C. A., Owens, C. P., Chim, N., Morse, R. P., McMath, L. M., Iniguez, A., Kimmey, J. M., Sawaya, M. R., Whitelegge, J. P., Horwitz, M. A., and Goulding, C. W. (2011) Discovery and characterization of a unique mycobacterial heme acquisition system. *Proc. Natl. Acad. Sci. U.S.A.* **108,** 5051–5056
21. Owens, C. P., Du, J., Dawson, J. H., and Goulding, C. W. (2012) Characterization of heme ligation properties of Rv0203, a secreted heme binding protein involved in *Mycobacterium tuberculosis* heme uptake. *Biochemistry* **51,** 1518–1531
22. Turlin, E., Débarbouillé, M., Augustyniak, K., Gilles, A. M., and Wandersman, C. (2013) *Staphylococcus aureus* FepA and FepB proteins drive heme iron utilization in *Escherichia coli*. *PLoS One* **8,** e56529
23. Dawson, R. M. C. (1986) *Data for Biochemical Research*, 3rd Ed., Clarendon Press, Oxford
24. Sil, S., Bose, T., Roy, D., and Chakraborti, A. S. (2004) Protoporphyrin IX-induced structural and functional changes in human red blood cells, haemoglobin and myoglobin. *J. Biosci.* **29,** 281–291
25. Ogola, H. J., Kamiike, T., Hashimoto, N., Ashida, H., Ishikawa, T., Shibata, H., and Sawa, Y. (2009) Molecular characterization of a novel peroxidase from the cyanobacterium *Anabaena* sp. strain PCC 7120. *Appl. Environ. Microbiol.* **75,** 7509–7518
26. Chance, B., and Maehly, A. C. (1955) Assay of catalases and peroxidases. *Methods Enzymol.* **2,** 755–764
27. Rahmanpour, R., and Bugg, T. D. (2013) Assembly *in vitro* of *Rhodococcus jostii* RHA1 encapsulin and peroxidase DypB to form a nanocompartment. *FEBS J.* **280,** 2097–2104
28. Shin, K.-S., and Lee Y-J. (2000) Purification and characterization of a new member of the laccase family from the white-rot basidiomycete *Coriolus hirsutus*. *Arch. Biochem. Biophys.* **384,** 109–115
29. Bannantine, J. P., and Stabel, J. R. (2001) Identification of two *Mycobacterium avium* subspecies paratuberculosis gene products differentially recognised by sera from rabbits immunised with live mycobacteria but not heat-killed mycobacteria. *J. Med. Microbiol.* **50,** 795–804
30. Lee, B. Y., Hefta, S. A., and Brennan, P. J. (1992) Characterization of the

major membrane protein of virulent *Mycobacterium tuberculosis*. *Infect. Immun.* **60,** 2066–2074

31. Khare, G., Gupta, V., Nangpal, P., Gupta, R. K., Sauter, N. K., and Tyagi, A. K. (2011) Ferritin structure from *Mycobacterium tuberculosis*: comparative study with homologues identifies extended C-terminus involved in ferroxidase activity. *PLoS One* **6,** e18570

32. Schneider, C. A., Rasband, W. S., and Eliceiri, K. W. (2012) NIH Image to ImageJ: 25 years of image analysis. *Nat. Methods* **9,** 671–675

33. Brown, M. E., Barros, T., and Chang, M. C. (2012) Identification and characterization of a multifunctional dye peroxidase from a lignin-reactive bacterium. *ACS Chem. Biol.* **7,** 2074–2081

34. Liu, X., Du, Q., Wang, Z., Zhu, D., Huang, Y., Li, N., Wei, T., Xu, S., and Gu, L. (2011) Crystal structure and biochemical features of EfeB/YcdB from *Escherichia coli* O157: ASP235 plays divergent roles in different enzyme-catalyzed processes. *J. Biol. Chem.* **286,** 14922–14931

35. Roberts, J. N., Singh, R., Grigg, J. C., Murphy, M. E., Bugg, T. D., and Eltis, L. D. (2011) Characterization of dye-decolorizing peroxidases from *Rhodococcus jostii* RHA1. *Biochemistry* **50,** 5108–5119

36. Dunford, H. B. (1999) *Heme Peroxidases*, p. 15, John Wiley & Sons, Inc., New York

37. Koduri, R. S., and Tien, M. (1995) Oxidation of guaiacol by lignin peroxidase: role of veratryl alcohol. *J. Biol. Chem.* **270,** 22254–22258

38. Gupta, V., Gupta, R. K., Khare, G., Salunke, D. M., and Tyagi, A. K. (2009) Crystal structure of Bfr A from *Mycobacterium tuberculosis*: incorporation of selenomethionine results in cleavage and demetallation of haem. *PLoS One* **4,** e8028

39. McMath, L. M., Contreras, H., Owens, C. P., and Goulding, C. W. (2013) The structural characterization of bacterioferritin, BfrA, from *Mycobacterium tuberculosis*. *J. Porphyrins Phthalocyanines* **17,** 229–239

40. Singh, R., Grigg, J. C., Armstrong, Z., Murphy, M. E., and Eltis, L. D. (2012) Distal heme pocket residues of B-type dye-decolorizing peroxidase: arginine but not aspartate is essential for peroxidase activity. *J. Biol. Chem.* **287,** 10623–10630

41. Jones, C. M., and Niederweis, M. (2011) *Mycobacterium tuberculosis* can utilize heme as an iron source. *J. Bacteriol.* **193,** 1767–1770

42. Chim, N., Iniguez, A., Nguyen, T. Q., and Goulding, C. W. (2010) Unusual diheme conformation of the heme-degrading protein from *Mycobacterium tuberculosis*. *J. Mol. Biol.* **395,** 595–608

43. Nambu, S., Matsui, T., Goulding, C. W., Takahashi, S., and Ikeda-Saito, M. (2013) A new way to degrade heme: the *Mycobacterium tuberculosis* enzyme MhuD catalyzes heme degradation without generating CO. *J. Biol. Chem.* **288,** 10101–10109

44. McMath, L. M., Habel, J. E., Sankaran, B., Yu, M., Hung, L. W., and Goulding, C. W. (2010) Crystallization and preliminary X-ray crystallographic analysis of a *Mycobacterium tuberculosis* ferritin homolog, BfrB. *Acta Crystallogr. Sect. F. Struct. Biol. Cryst. Commun.* **66,** 1657–1661

45. Mishra, S., and Imlay, J. (2012) Why do bacteria use so many enzymes to scavenge hydrogen peroxide? *Arch. Biochem. Biophys.* **525,** 145–160

46. Manca, C., Paul, S., Barry, C. E., 3rd, Freedman, V. H., and Kaplan, G. (1999) *Mycobacterium tuberculosis* catalase and peroxidase activities and resistance to oxidative killing in human monocytes in vitro. *Infect. Immun.* **67,** 74–79

47. Liu, X., and Theil, E. C. (2004) Ferritin reactions: direct identification of the site for the diferric peroxide reaction intermediate. *Proc. Natl. Acad. Sci. U.S.A.* **101,** 8557–8562

48. Choudhary, S., Quin, M. B., Sanders, M. A., Johnson, E. T., and Schmidt-Dannert, C. (2012) Engineered protein nano-compartments for targeted enzyme localization. *PLoS One* **7,** e33342

49. Kerfeld, C. A., Heinhorst, S., and Cannon, G. C. (2010) Bacterial microcompartments. *Annu. Rev. Microbiol.* **64,** 391–408

50. Yeates, T. O., Crowley, C. S., and Tanaka, S. (2010) Bacterial microcompartment organelles: protein shell structure and evolution. *Annu. Rev. Biophys.* **39,** 185–205

51. Jorda, J., Lopez, D., Wheatley, N. M., and Yeates, T. O. (2013) Using comparative genomics to uncover new kinds of protein-based metabolic organelles in bacteria. *Protein Sci.* **22,** 179–195

52. Fan, C., Cheng, S., Liu, Y., Escobar, C. M., Crowley, C. S., Jefferson, R. E., Yeates, T. O., and Bobik, T. A. (2010) Short N-terminal sequences package proteins into bacterial microcompartments. *Proc. Natl. Acad. Sci. U.S.A.* **107,** 7509–7514

53. Akita, F., Chong, K. T., Tanaka, H., Yamashita, E., Miyazaki, N., Nakaishi, Y., Suzuki, M., Namba, K., Ono, Y., Tsukihara, T., and Nakagawa, A. (2007) The crystal structure of a virus-like particle from the hyperthermophilic archaeon *Pyrococcus furiosus* provides insight into the evolution of viruses. *J. Mol. Biol.* **368,** 1469–1483

54. Wikoff, W. R., Liljas, L., Duda, R. L., Tsuruta, H., Hendrix, R. W., and Johnson, J. E. (2000) Topologically linked protein rings in the bacteriophage HK97 capsid. *Science* **289,** 2129–2133

55. Sherman, D. R., Voskuil, M., Schnappinger, D., Liao, R., Harrell, M. I., and Schoolnik, G. K. (2001) Regulation of the *Mycobacterium tuberculosis* hypoxic response gene encoding α-crystallin. *Proc. Natl. Acad. Sci. U.S.A.* **98,** 7534–7539

56. Garbe, T. R., Hibler, N. S., and Deretic, V. (1999) Response to reactive nitrogen intermediates in *Mycobacterium tuberculosis*: induction of the 16-kilodalton α-crystallin homolog by exposure to nitric oxide donors. *Infect. Immun.* **67,** 460–465

57. Voskuil, M. I., Visconti, K. C., and Schoolnik, G. K. (2004) *Mycobacterium tuberculosis* gene expression during adaptation to stationary phase and low-oxygen dormancy. *Tuberculosis* **84,** 218–227

58. Czekster, C. M., and Blanchard, J. S. (2012) One substrate, five products: reactions catalyzed by the dihydroneopterin aldolase from *Mycobacterium tuberculosis*. *J. Am. Chem. Soc.* **134,** 19758–19771

59. Lassila, J. K., Bernstein, S. L., Kinney, J. N., Axen, S. D., and Kerfeld, C. A. (2014) Assembly of robust bacterial microcompartment shells using building blocks from an organelle of unknown function. *J. Mol. Biol.* **426,** 2217–2228

60. Rustad, T. R., Harrell, M. I., Liao, R., and Sherman, D. R. (2008) The enduring hypoxic response of *Mycobacterium tuberculosis*. *PLoS One* **3,** e1502

61. Boshoff, H. I., Myers, T. G., Copp, B. R., McNeil, M. R., Wilson, M. A., and Barry, C. E., 3rd (2004) The transcriptional responses of *Mycobacterium tuberculosis* to inhibitors of metabolism: novel insights into drug mechanisms of action. *J. Biol. Chem.* **279,** 40174–40184

62. Corchero, J. L., and Cedano, J. (2011) Self-assembling, protein-based intracellular bacterial organelles: emerging vehicles for encapsulating, targeting and delivering therapeutic cargoes. *Microb. Cell Fact.* **10,** 92

63. Marchler-Bauer, A., Lu, S., Anderson, J. B., Chitsaz, F., Derbyshire, M. K., DeWeese-Scott, C., Fong, J. H., Geer, L. Y., Geer, R. C., Gonzales, N. R., Gwadz, M., Hurwitz, D. I., Jackson, J. D., Ke, Z., Lanczycki, C. J., Lu, F., Marchler, G. H., Mullokandov, M., Omelchenko, M. V., Robertson, C. L., Song, J. S., Thanki, N., Yamashita, R. A., Zhang, D., Zhang, N., Zheng, C., and Bryant, S. H. (2011) CDD: a Conserved Domain Database for the functional annotation of proteins. *Nucleic Acids Res.* **39,** D225–D229